JBC RESEARCH ARTICLE

Magnesium-dependent-protein phosphatase 1B regulates the protein arginine methyltransferase 5 through the modulation of myosin phosphatase

Received for publication, July 10, 2024, and in revised form, December 8, 2024 Published, Papers in Press, December 18, 2024,
https://doi.org/10.1016/j.jbc.2024.108107

Ilka Keller, Ádám Ungvári, Evelin Major, Dániel Horváth, Zoltán Kónya, Emese Tóth, Ferenc Erdődi, Andrea Kiss, and Beáta Lontay*

From the Department of Medical Chemistry, Faculty of Medicine, University of Debrecen, Debrecen, Hungary

Reviewed by members of the JBC Editorial Board. Edited by Philip A. Cole

Dysregulation of the expression levels and the activity of kinases/phosphatases is an intrinsic hallmark of tumor transformation and progression, as either as a primary cause or consequence. The myosin phosphatase (MP)/protein arginine methyltransferase 5 (PRMT5)/histone (H4) pathway is an oncogenic signaling pathway downregulating the gene expression of tumor suppressors. However, the upstream regulators of the pathway are unknown. We show that the Mg^{2+}-dependent protein phosphatase 1 B (PP2Cb or PPM1B) interacts and regulates MP through the MYPT1 regulatory subunit, and this interplay results in the inactivation of the tumorigenic pathway driven by PRMT5. The phospho-Thr696 inhibitory residues of the MYPT1 regulatory subunit of MP was dephosphorylated by PPM1B. The inhibition of PPM1B by sanguinarine resulted in the deactivation of MP and the increased activity of PRMT5 leading to increased symmetric dimethylation of histone H4 in HeLa cells. The overexpression of the PPM1B had the opposite action. The overexpression of PPM1B decreased the colonization activity of HeLa cells through modulation of MP. Finally, human cervical carcinoma biopsies showed almost complete elimination of PPM1B compared to their healthy control counterparts. The phosphorylation of the inhibitory $MYPT1^{pT696}$ and the regulatory $PRMT5^{pT80}$ residues and the symmetric dimethylation of H4 were elevated in the cancer biopsies and it resulted in a decrease in retinoblastoma protein expression. The results indicate a tumor suppressor role of the PPM1B/MP axis *via* inhibition of PRMT5, thereby regulating gene expression through H4 arginine dimethylation. Collectively, PPM1B is a tumor suppressor and a possible tumor marker for cervical carcinoma.

Oncogenesis is a complex process associated with accumulation of genetic and epigenetic defects and converged into aberrant regulation of intracellular and extracellular signaling pathways leading to the alteration of the transcriptional program (1). High throughput "omics" analysis of gene expression in cancer patients led to the identification of key genes and signaling pathways that drive cancer progression (2, 3). However, relatively little is known about the mechanisms that underlie the deregulation of signaling pathways in cancers.

One of the oncogenic signaling pathways is the myosin phosphatase (MP)/protein arginine methyltransferase 5 (PRMT5)/histone pathway downregulating the gene expression of tumor suppressors (4). Arginine-methylated proteins function in a number of key cellular processes required for maintenance of tissue homeostasis as well as disease phenotypes such as cancer and catalyzed by protein arginine methyltransferases (5). Methylation modifies the hydrogen bonding of the side chain of the targeted protein arginine amino acid, resulting in changes in protein function and molecular properties (5). PRMT5 is the major enzyme that catalyzes specifically symmetric dimethylation by using S-adenosylmethionine as a methyl donor (6). In human cells, PRMT5 performs its methylation activity as part of a heterooctameric methylosome enzyme complex that consists of four PRMT5 and four methylosome protein 50 (MEP50), which, in addition to stabilizing PRMT5, contributes to its activity by targeting its substrates to the holoenzyme and functions as a positive allosteric regulator (7, 8). Substrates for the enzyme include transcriptional regulators (*e.g.* tumor protein p53 (p53), E2F transcription factor 1 (E2F1), tumor protein p65 (p65), Kruppel like factor 4 (KLF4), sterol regulatory element binding protein (SREBP1) and molecules involved in signal transduction (*e.g.* epidermal growth factor receptor and platelet-derived growth factor receptor) and by symmetrically dimethylating some Sm proteins present in snRNP complexes (*e.g.* small nuclear ribonucleoprotein-associated protein B (SmB) and small nuclear ribonucleoprotein-associated protein D1 (SmD1)), thereby PRMT5 contributes to the maturation of mRNA by promoting their splicing. However, its most important substrates are histone proteins, of which it performs symmetric dimethylation on arginine 8 of H2A and arginine 3 of H3 and H4, leading to epigenetic modification and regulating the expression of several genes implicated in both tumor promotion and suppression (5). These include tumor suppressor genes (*e.g.* retinoblastoma protein (pRb), p53, protein tyrosine phosphatase B and protooncogenes (*e.g.* ras-proximate-1 (RAP), mitogen-activated protein kinase (MAPK) (9). In several types of tumors, overactivation of PRMT5 protein has

* For correspondence: Beáta Lontay, lontay@med.unideb.hu.

been described, resulting in silencing of the tumor suppressors (4, 10).

Several phosphorylation sites involved in the PRMT5 regulation have been described. These include phosphorylation of the side chains Tyr297, Tyr304, and Tyr306 by the mutant kinase janus kinase 2 (JAK2), which inhibits the formation of the methylosome complex by interfering with the interaction of PRMT5 with methylosome protein 50, thereby reducing the methylation of histone proteins. This, in turn, contributes to the development of myeloproliferative diseases (11, 12). Our group has described another phosphorylation site, Thr80, in hepatocellular carcinoma samples. The site is phosphorylated by Rho A activated kinase (ROK) and dephosphorylated by MP, the former therefore activates and the latter inhibits PRMT5 (4).

MP is a Ser/Thr specific protein phosphatase composed of protein phosphatase catalytic subunit β isoform (PP1β/δ or PPP1CB or PP1 catalytic subunit (PP1c)) and a myosin phosphatase target subunit 1 (MYPT1) regulatory subunit (MYPT1 or PPP1R12A) that determines the substrate specificity of the enzyme (13). MP is a key enzyme involved not only in the regulation of the activity of myosin in muscle contraction and cell motility, but in various cellular processes other substrates have also been identified (14). Phosphorylation of MYPT1 on Ser/Thr residues by a variety of protein Ser/Thr kinases is one of the principal regulatory mechanisms of MP's functions causing activation or inhibition of this enzyme. There are two major and well-characterized inhibitory sites in MYPT1, namely Thr696 and Thr853 (15). ROK was first identified as the kinase for the phosphorylation of both inhibitory phosphorylation sites [19], but later several other kinases including zipper-interacting protein kinase (ZIPK), integrin-linked kinase (ILK), myotonic dystrophy kinase, protooncogene serine/threonine-protein kinase (Raf-1 [20] and p21-activated protein kinases were also shown to act on Thr696 (16). Phosphorylation of MYPT1 on Thr696 or on Thr853 attenuated the activity of MP by inducing structural movements that allows the interaction of the inhibitory phosphorylated region of MYPT1 with the substrate binding groove of the catalytic center of PP1c. The role of the MYPT Thr853 phosphorylation site in the regulation of the MP holoenzyme is not clear. Some of the studies found that MYPT1 Thr853 phosphorylation does not inhibit MP activity in smooth muscle (16), while others described an equivalent effect with the phosphorylation of MYPT1 at Thr696 and found the MYPT1 Thr853 as a primary ROK phosphorylation site using a ROK-selective inhibitor (17). *Khasnis at al* suggested that the phosphorylation at Thr696 facilitated the phosphorylation at Thr853 in ileal smooth muscle (18). The phosphorylation of the two sites appears to be independent and each site is accessible to a different kinase(s) and there is also the possibility that in different cells the accessibility of these two sites to distinct kinases may vary (17, 19) but based on the contradictory data, we focused on the role of MYPT1 Thr696, the major MP regulatory site, in our study.

Since only MP and PRMT5 but not ROK, the upstream regulator of these enzymes, shows nuclear localization, the question arose as to what the upstream regulator of the MP/PRMT5/histone signal transduction pathway is. Based on our previous findings several proteins in the MYPT1 nuclear interactome have been described in addition to histone and the members of methylosome complex. Strikingly, the only MYPT1 interacting partner with catalytic activity identified by mass spectrometry analysis was $Mg^{2+/}Mn^{2+}$ -dependent protein phosphatase 1 B isoform (PPM1B or PP2C beta isoform or PP2Cβ) (20). Therefore, we aimed to investigate the role of this PPM1B in the regulation of the oncogenic signaling regulated by PRMT5.

Results

Interaction of PPM1B with MYPT1

Initial reports have already described the presence of MP in the nucleus and its role in the regulation of gene expression through the dephosphorylation of PRMT5 (4, 14). However, there is no information about the upstream regulators of MP in the nucleus. One of the candidates is the Mg^{2+}/Mn^{2+}-dependent protein phosphatase 1B (PPM1B) but its exact function and correlation to the MP/PRMT5/histone proto-oncogene axis remained unknown. PPM1B was reported as an interacting protein of MYPT1 when GST-MYPT1 pull-down fraction was analyzed by mass spectrometry [20], and it was the only potential MYPT1 regulating enzyme in the MYPT1-interactome. Our goal was to further support our omics-related data on the interaction between PPM1B and the MYPT1 subunit, and we carried out reciprocal immunoprecipitations (Fig. 1*A*), pull-down assays (Fig. 1*B*), and Duolink proximity ligation assay (Fig. 1*C*).

First, an immunoprecipitation assay was conducted by using FT-PPM1B and FT-MYPT1 overexpressing tsA201 cell lysates with anti-MYPT1 and anti-PPM1B antibodies. MYPT1 and PPM1B were coprecipitated and the interaction was documented in the PPM1B precipitate; however, PPM1B was also presented in the FT-MYPT1 precipitate. Protein A sepharose (PAS) bead crosslinked with anti-MYPT1 coprecipitate both MYPT1 and PPM1B, but PAS bead cross-linked with PPM1B antibody did not presented binding of MYPT1, which might be explained by the overlap of the PPM1B binding region of MYPT1 with the anti-MYPT1 antibody epitope. Since the Mg^{2+}/Mn^{2+}-dependent protein phosphatase 1 A (PPM1A) shows the highest sequence homology with PPM1B, and one out of the six identified peptides in the MYPT1 interactome presented 100% homology with PPM1A isoform, we also assayed the immunoprecipitate for PPM1A (Fig. 1*A*). Based on our result, although all the investigated proteins were present in the input lysates, PPM1A did not show protein-protein interaction with MYPT1.

Second, to further support the interaction between PPM1B and MYPT1, pull-down assays were also carried out using GST-MYPT1 or GST (as negative control). Untransfected or FT-PPM1B overexpressed tsA201 lysates, or recombinant PP1c as positive controls were applied. The GST and GST-MYPT1 binding proteins were eluted from the Glutathione Sepharose beads, separated by SDS-PAGE and assayed by

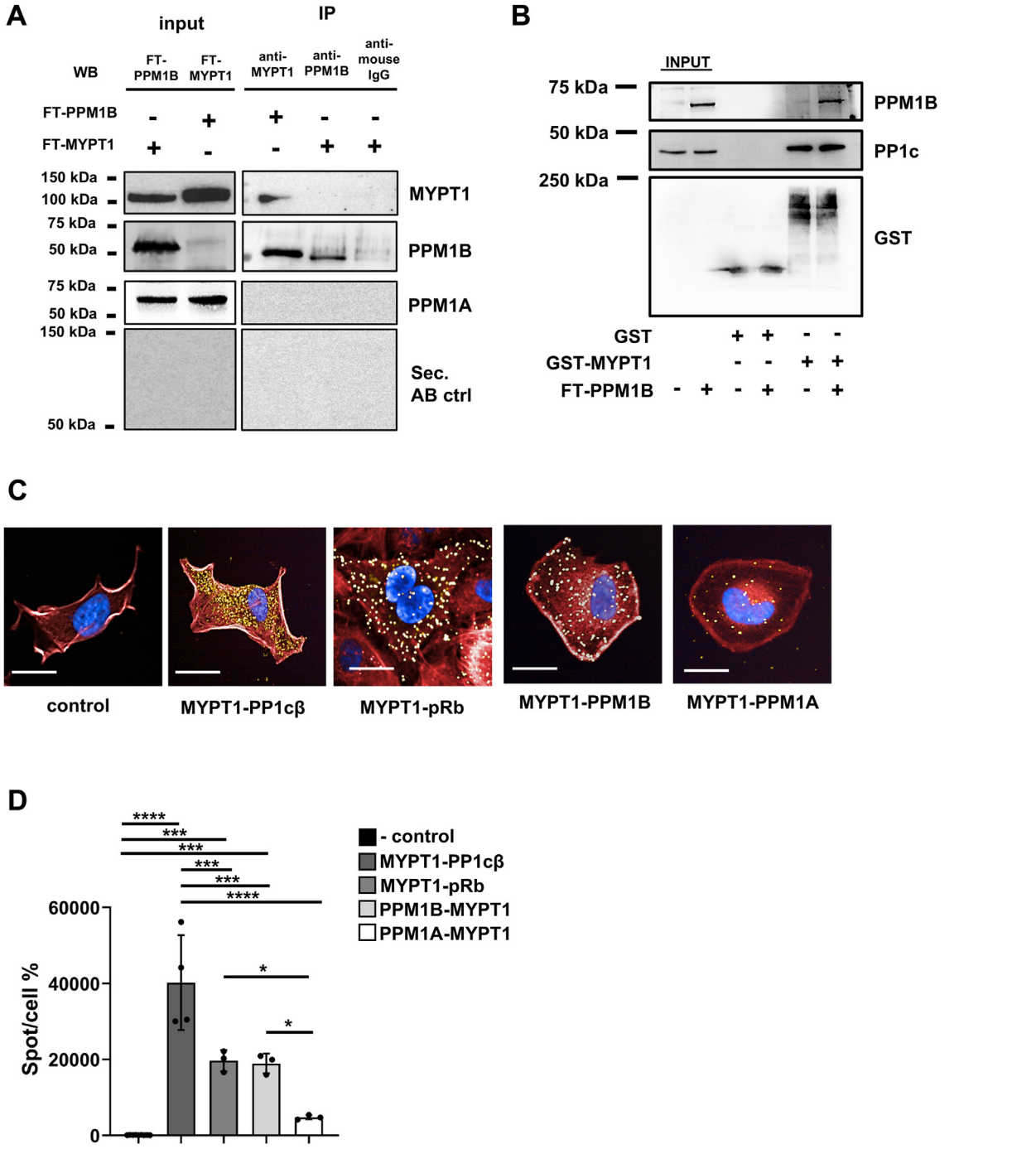

Figure 1. Protein-protein interaction of PPM1B and MYPT1. *A*, immunoprecipitation was performed from tsA201 cell lysate with antibodies specific for MYPT1 and PPM1B and coupled to Protein-A sepharose, and the precipitates were analyzed by Western blot using the indicated antibodies. *B*, pull-down of Flag-PPM1B by GST-MYPT1. GST, or GST-MYPT1 coupled glutathione-sepharose 4B beads were incubated with untransfected or Flag-PPM1B overexpressing tsA201 cell lysates. The interaction was detected by Western blot analysis using anti-GST and anti-Flag antibodies. PP1cβ was identified as a positive control using anti-PP1c antibody. *C*, quantitative analysis of MYPT1 and PPM1B interactions evaluated by Duolink protein-protein interaction assay. Antibodies against the retinoblastoma protein (pRb) were applied as positive control. Interaction of MYPT1 was assayed with PPM1A antibody, as well. F-actin was stained by Alexa688 Phalloidin (*red*), nuclei were visualized by DAPI (*blue*). Protein-protein interaction is indicated as a *yellow* signal. The scale bar represents 10 μm. *D*, bars represent spots/cell. Negative control group value was taken as a 100%, and all other groups are expressed as a ratio. Values represents mean ± SD; n = 3 to 9; groups were compared by one way ANOVA followed by Tukey *post hoc* test, where (*) $p < 0.05$, $p < 0.01$ (**), $p < 0.001$ (***) and $p \leq 0.0001$ (****).DAPI, 4′,6-diamidino-2-phenylindole; MYPT1: myosin phosphatase target subunit 1, PPM1B: protein phosphatase, Mg^{2+}/Mn^{2+} -dependent 1 B or PP2Cβ.

Western blot analysis using antibodies against GST, PP1c, and PPM1B. GST-MYPT1 but no GST showed interaction with PPM1B and the interaction between the subunits of MP, namely PP1c and MYPT1 was verified (Fig. 1*B*). Third, the interaction of PPM1B with MYPT1 was analyzed in HeLa human cervical carcinoma cells by Duolink proximity ligation assay (PLA) (Fig. 1, *C* and *D*). Samples labeled with anti-MYPT1 and anti-PP1β antibodies (specific for PP1β catalytic

subunit of MP) served as positive control showing the interaction of the holoenzyme. We also presented the interaction between MYPT1 and its already known interacting partner and the substrate of MP, the pRb as another positive control. For investigating PPM1B-MYPT1 interaction, samples were incubated with anti-MYPT1 and anti-PPM1B antibodies, while unlabeled group acted as negative control (Fig. 1*C*). The negative control spot number normalized to cell number was considered as 100%, to which we compared the values of interaction between PP1c and MYPT1, pRb, and MYPT1, as well as PPM1B and MYPT1. The analysis proved the mutual and strong interaction between the subunits of the MP holoenzyme and revealed a significant number of interactions per cell between not only the pRb (the substrate of MP) and MYPT1 (p = 0.0004) but also between PPM1B and MYPT1 (p = 0.0006) in total cell area compared to negative control (Fig. 1*D*). To elucidate the difference in the interaction between MYPT1 and PPM1B and MYPT1 and PPM1A, an interaction group labeled with anti-MYPT1 and anti-PPM1A antibodies were also established, which shown no significant spot number per cell compared to negative control group (p =) (Fig. 1*D*). In addition, the degree of interaction between PPM1A and MYPT1 was significantly lower (p = 0.0363) compared to the PPM1B-MYPT1 interaction. We found no difference in the spot number per cell between the PPM1A-MYPT1 group compared to the negative control (p = 0.7012) (Fig. 1*D*) All these data verify the interaction between MYPT1 and PPM1B and indicate their localization and interaction not exclusively in the nucleus but in the cytoplasm, as well.

MP is the substrate of PPM1B

To prove the regulatory role of PPM1B on MP through the regulation of its MYPT1 subunit, GST-MYPT1 was phosphorylated by ROK, and *in vitro* phosphatase assay was carried out using recombinant PPM1B (Fig. 2*A*). Western blot data using anti-MYPT1^{pT696} showed that ROK successfully phosphorylated the inhibitory sites, and the relative phosphorylation of Thr696 residues increased by 8.61-fold (p = 0.0004) compared to GST-MYPT1 group. Addition of recombinant, purified, enzymatically active PPM1B caused a substantial decrease in the phosphorylation of MYPT^{pT696} and from a relative value 1.99 to 0.404 (p = 0.0031) (4.8-fold decrease) indicating that phospho-MYPT1 is a substrate of PPM1B. To assess the PPM1B activity sanguinarine (SNG)-dependency, we completed our phosphatase assay with or without the addition of 1 μM SNG to the assay. The phosphorylation of MYPT1 at the Thr696 inhibitory residues showed 2.76-fold (p = 0.0062) elevation compared to ROK and PPM1B-treated samples. The Thr696 phosphorylation level of SNG treated samples was significantly different from only the ROK-phosphorylated ones. To investigate the Mn^{2+}/Mg^{2+} ion dependency of PPM1B, we repeated the experiments without Mn^{2+} and Mg^{2+} ions. The phosphorylation of MYPT1 at Thr696 increased 2.738-fold (p = 0.006) compared to ROK- and PPM1B-treated group. The MP activity in HeLa cell lysates was quantified upon PPM1B inhibition using SNG that is a plant benzo(c)phenanthridine alkaloid, which was identified as a potent and specific inhibitor of PPM1 enzymes (21). SNG was applied on cell culture system since there is no commercially available PPM1B-specific inhibitor and it was

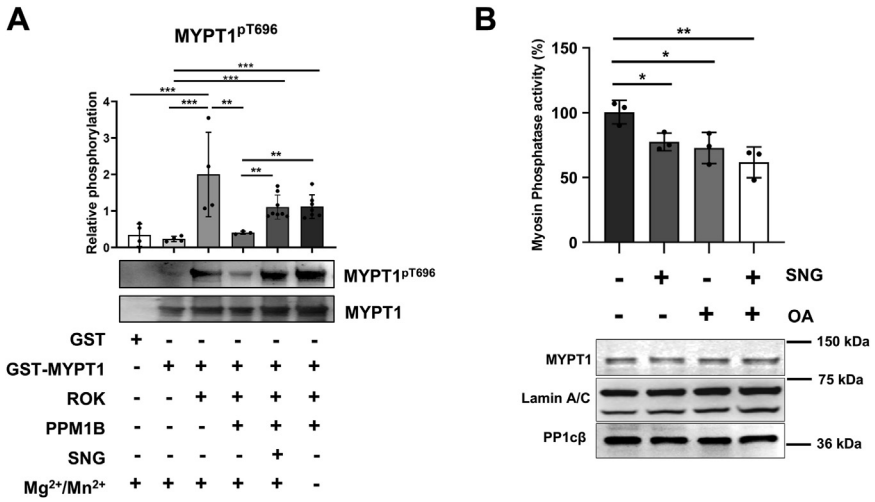

Figure 2. PPM1B activates MP by dephosphorylating Thr696 and Thr853 inhibitory phosphorylation of MYPT1. Purified GST or GST-MYPT1 were coupled with glutathione-sepharose 4B beads. Resin-bound GST-MYPT1 was phosphorylated by ROK, and then incubated with PPM1B in the presence of Mg^{2+} and Mn^{2+} ions, or Mg^{2+} and Mn^{2+} ions plus 1 μM sanguinarine, or in the absence of Mg^{2+} and Mn^{2+}. Phosphorylation of GST-MYPT1 was tested by Western blot using anti-MYPT1-^{pT696} antibody (*A*). The amount of GST-MYPT1 in each sample was detected by anti-MYPT1 antibody. Multiple columns were compared by one-way ANOVA followed by Tukey *post hoc* test, two columns were compared by unpaired two-tailed *t* test, where $p < 0.05$ (*), $p < 0.01$ (**) and $p < 0.001$ (***).Columns represent mean ± SD, n = 3 to 11. *B*, HeLa cells were treated with 1 μM SNG or 50 nM OA, or with their combination. Myosin phosphatase activity was assessed using 1 μM ^{32}P-myosin substrate. The liberated $^{32}P_i$ of the samples were measured and normalized to the MYPT1 protein content calculated by a calibration curve using GST-MYPT1 recombinant protein and displayed as percent values of the control counts (100%). Values represent mean ± SD; n = 3. Groups were compared using one way ANOVA followed by Tukey *post hoc* test, where $p < 0.05$ (*) and $p < 0.01$ (**). Cell lysates were assessed by Western blot analysis for MYPT1, PP1cβ, and lamin A/C as loading control. MP, myosin phosphatase; MYPT1: myosin phosphatase target subunit 1; OA, okadaic acid; PP1c, PP1 catalytic subunit; PPM1B: protein phosphatase, Mg^{2+}/Mn^{2+} -dependent 1 B or PP2Cβ; ROK, Rho A activated kinase; SNG, sanguinarine.

widely applied for the inhibition of PPM1B. *Yu et al., 2020* (22), showed that 4 μM SNG treatment for 24 h significantly inhibited cell proliferation and promoted apoptosis of THP-1 cells. *Aburai et al., 2010* (21), also showed an increased caspase 3/7 activity upon 1 μM SNG treatment even after 6 h. Therefore, it was necessary to conduct experiments on the effect of SNG on HeLa cells. Fig. S2*A* shows a 11.42% (p = 0.0105) reduction in the viability of HeLa cells upon 1 μM SNG treatment for 60 min by Alamar Blue assay.

Phosphatase activity in the HeLa lysates was assayed using gizzard ^{32}P-myosin as substrate (23) (Fig. 2*B*). Previously, it was shown that MYPT1 dramatically increases the activity of PP1c toward phosphorylated myosin and it is accepted that smooth muscle myosin (or heavy-meromyosin) is effectively dephosphorylated only by the MP holoenzyme in cell lysates or tissue extracts (24). Therefore, assays conducted using ^{32}P-myosin should reflect only the MP activity. In our assay, none of the subunits of the MP holoenzyme showed a change in the protein content (Fig. 1*B* immunoblots). Fig. 2*B*. illustrates that upon inhibition of PPM1 with SNG the MP activity, that was normalized to the MYPT1 content of the cell lysate, decreased by 23% (p = 0.02) compared to the control untreated samples indicating the involvement of PPM1B in the regulation of MP activity. Treatments with okadaic acid (OA), the potent protein phosphatase 1 and 2A inhibitor toxin, induced a 29% reduction (p = 0.04) in the total MP activity in HeLa cells and the combined application of the inhibitors appeared to be additive showing a 40% decrease (p = 0.007) compared to the untreated control. Briefly, 50 nM OA only inhibits protein phosphatase-2A (PP2A), and PP1 is not influenced (25), and PP1 activity in cells was not affected even with 1 μM OA (26). Therefore, we assume that the MP holoenzyme, containing PP1c is not influenced directly but indirectly through other phosphatase such as protein phosphatase-2A (PP2A) and PPM1B dephosphorylating the MYPT1 subunit.

PPM1B inhibition results in increased phosphorylation of the MYPT1 inhibitory phosphorylation sites in the subcellular fractions of HeLa cells

To validate the *in vivo* regulatory effect of PPM1B on MP, HeLa cells were treated with 1 μM SNG to inhibit the activity of PPM1B. Since the interaction was suggested to be mainly nuclear, subcellular fractions of the vehicle and SNG-treated cells were generated to gain total cell lysate, cytoplasmatic, and nuclear fractions. Furthermore, to exclude the effect of SNG on the PPM1B expression and localization, total cell lysate, nuclear and cytosolic fractions of HeLa cells were prepared with or without SNG treatment, and significant changes in the expression was not observed in any experimental condition either by Western blot analysis in subcellular fractions (Fig. S2*B*) or by immunofluorescent staining (Fig. S2*C*). The purity of the fractions was validated in each case by tubulin and lamin A/C as cytoplasmic and nuclear markers, respectively. Based on our results, SNG did not affect PPM1B expression and localization in HeLa cells. The effect of 1 μM SNG was also assessed by semiquantitative Western blot analysis. SNG had no effect on the expression of MYPT1 but elevated the amount of nuclear MYPT1 by 1.58-fold (p = 0.0233) suggesting the translocation of the enzyme into the nucleus upon PPM1B inhibition (Fig. 3*A*). This effect was also verified by immunofluorescent staining (Fig. 3*B*) where MYPT1 was present with a higher intensity in the 4′,6-diamidino-2-phenylindole (DAPI) labeled area of HeLa cells. We also investigated the phosphorylation of the T696 residue of MYPT1 (Fig. 3*C*), and it was elevated upon SNG-treatment in the total lysates by 2.048-fold (p = 0.0119). The nuclear phosphorylation was significantly elevated at MYPT1^{pT696} upon SNG treatment by 2.137-fold (p = 0.0201) (Fig. 3*C*) and the MYPT1^{pT696} fluorescent staining (green) also indicates a remarkable increase specifically in the nuclei (Fig. 3*D*). Concluding these observations, we suggest the translocation of MYPT1 from the cytoplasm to the nucleus as the results of the elevated phosphorylation level on Thr696 residue because of PPM1B inhibition (Fig. 3, *A* and *C*).

PPM1B inhibition by sanguinarine affects the PRMT5 activity and the gene expression

MP is known to inhibit PRMT5 by dephosphorylating its Thr80 regulatory residue (27). We examined the effect of PPM1B inhibition by SNG on the expression and post-translational modifications of PRMT5 and its substrate H4 in HeLa cells by semiquantitative Western blot analysis (Fig. 4, *A*, *C*, *E* and *G*) and immunofluorescent staining (Fig. 4, *B*, *D*, F and H). Our data demonstrate that expression of PRMT5 was not affected in any of the investigated cell fractions (Fig. A and B), but the Thr80 phosphorylation was significantly elevated in each of the examined cellular compartments upon the SNG treatment (Fig. 4, *C* and *D*). The relative phosphorylation level of PRMT5 at Thr80 elevated in the total cell lysates, cytoplasm as well as in the nuclear fraction by 1.96-fold (p = 0.0493), 1.5-fold (p = 0.0437), and 2.36-fold (p = 0.0208), respectively compared to untreated control sample upon SNG treatment (Fig. 4, *C* and *D*). We also examined H4 expression (Fig. 4, *E* and *F*), along with its symmetrical dimethylation (Fig. 4, *G* and *H*). In correlation with our previous findings, we have perceived elevated symmetrical dimethylation in total cell lysate by 1.54-fold (p = 0.0339), and elevation by 3.25-fold in the nuclear compartment (p = 0.0035) (Fig. 4, *G* and *H*) without any changes at gene expression level (Fig. 4, *E* and *F*).

Overexpression of FT-PPM1B impedes PRMT5 activity through the activation of myosin phosphatase

Since SNG inhibits all the members of the Mg^{2+}/Mn^{2+}-dependent phosphatases (21), and there are no commercially available selective inhibitors for PPM1B, we aimed to demonstrate specific effects related to the PPM1B isoform. The specific knockdown of this isoform was challenging and biologically questionable since its expression level was already decreased or almost eliminated in many cancer tissues compared to control ones (28). For this, the Flag-tagged PPM1B isoform was overexpressed in HeLa cells. The efficiency of PPM1B overexpression was validated by confocal

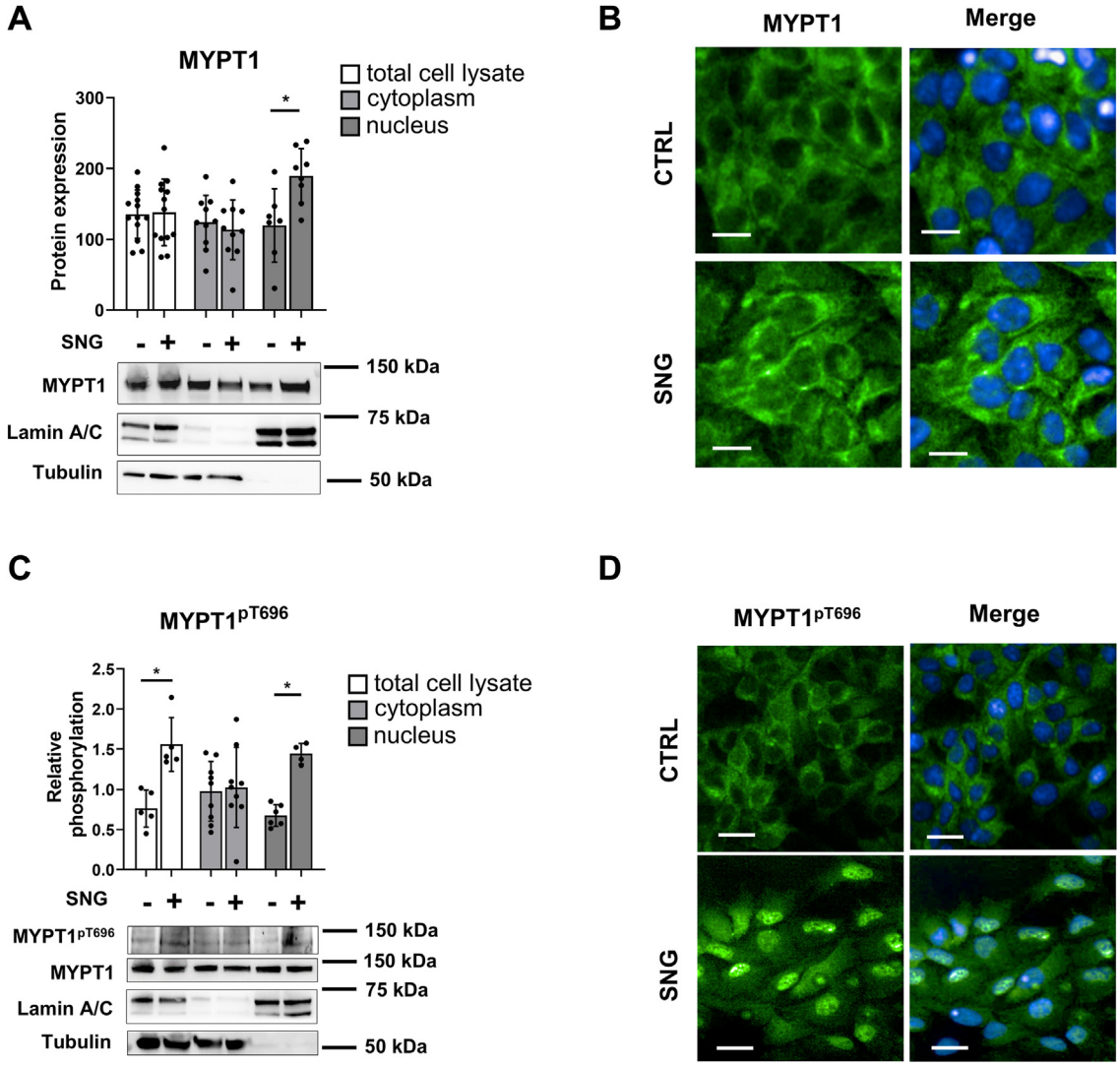

Figure 3. Effect of SNG on MYPT1 expression and MP activity in HeLa cells. Total cell lysates, nuclear and cytoplasmic fractions from control and SNG-treated cells were examined by Western blot analysis using anti-MYPT1 (*A*) and anti-MYPT1^{pT696} (*C*) antibodies. Values represent mean ± SD, n = 3 to 13. Columns display the expression of MYPT1, along with phosphorylation at MYPT1 ^{pT696} residue. For comparison of multiple groups two way ANOVA was used, followed by Tukey *post hoc* test, for comparison of two groups two tailed unpaired *t* test was used where $p < 0.05$ (*) and $p < 0.001$ (***). Immunofluorescent staining of control and SNG-treated HeLa cells using antibodies specific for MYPT1 (*B*) and MYPT1^{pT696} (*D*) are shown. Nuclei are stained with DAPI. The scale bar represents 10 μm. DAPI, 4′,6-diamidino-2-phenylindole; MP, myosin phosphatase; MYPT1: myosin phosphatase target subunit 1; SNG, sanguinarine.

microscopy, labeling Flag-tag with Alexa488 fluorophore (Fig. S3*D*) as well as by semiquantitative Western blot analysis using anti-Flag antibody (Fig. S3*B*), as well as anti-PPM1B antibody (Fig. S3*A*). Transfection evoked a significant decrease of viability of mock transfected cells compared to control by 25.25% ($p = 0.021$), but interestingly no significant viability changes were detectable between the control and PPM1B-overexpressing cells (Fig. S3*C*). Overexpression of PPM1B did not affect the expression of either MYPT1 (Fig. 5*A*) or PRMT5 (Fig. 5*C*) compared to HeLa cells transfected with empty vector, suggesting that PPM1B has no effect on their gene expression. On the other hand, upon PPM1B overexpression, Thr696 phosphorylation of MYPT1 exhibited a 0.7-fold ($p = 0.0425$) decrease compared to the mock control, and the transfection had no effect in any investigated cases on the phosphorylation levels. The downstream substrate of MP, PRMT5 showed a significant reduction by 0.61-fold ($p = 0.0158$) compared to the control, and a 0.68-fold decrease ($p = 0.0354$) compared to the mock, in the level of its Thr80 phosphorylation indicating that MYPT1 activity is indirectly correlated to PRMT5 activity and depends on PPM1B expression (Fig. 5*D*). Along with these findings, the major nuclear PRMT5 substrate, namely H4 and its symmetric dimethylation was investigated. While the protein level of histone proteins was not altered (Fig. 5*E*), the symmetric dimethylation of H4 decreased by 0.64-fold ($p = 0.0413$) and by 0.74-fold ($p = 0.0312$) comparing to control and mock transfected cells, respectively (Fig. 5*F*). Immunofluorescence staining was used to track the expression and posttranslational modification of MYPT1, PRMT5, and H4. The obtained results were consistent with those from Western blot analysis (Fig. S4, *A*–*G*).

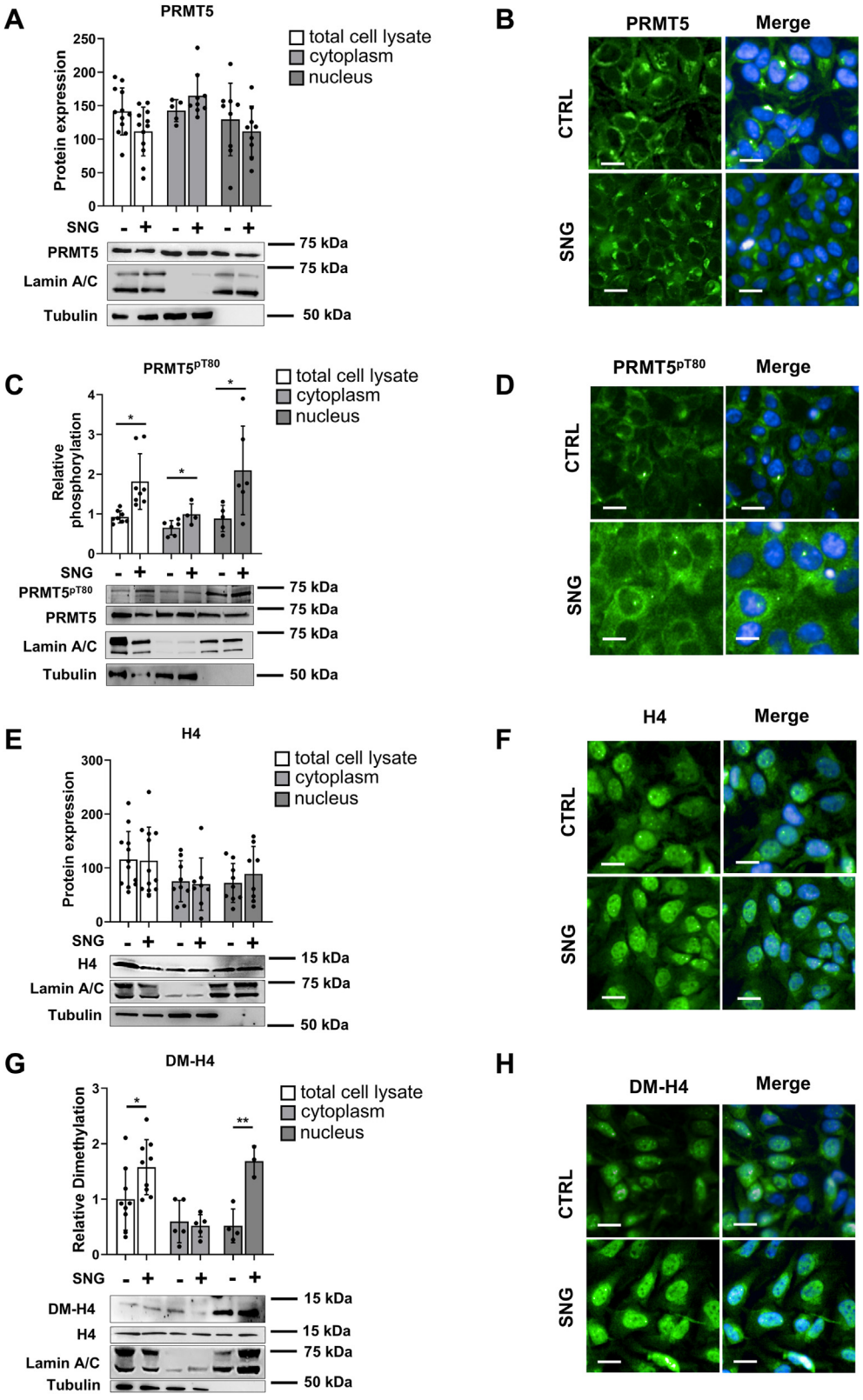

Figure 4. Effect of treatment by SNG on PRMT5 and H4 in HeLa cells revealed by Western blot. Total cell lysates, nuclear, and cytoplasmic fractions from control and SNG-treated cells were assessed by Western blot analysis using anti-PRMT5 (*A*), anti-PRMT5^{pT80} (*C*), anti-H4 (*E*) and anti-DM-H4 (*G*) antibodies. Values are mean ± SD, n = 3 to 12. Columns display the expression of PRMT5 and H4, along with phosphorylation at PRMT5^{T80} residue, and symmetric dimethylation of H4. For comparison of multiple groups two way ANOVA was used followed by Tukey *post hoc* test, or for comparison of two groups two tailed unpaired *t* test was used where $p < 0.05$ (*) and $p < 0.01$ (**). Immunofluorescent staining of control and SNG-treated HeLa cells using antibodies specific for PRMT5 (*B*), anti-PRMT5-P^{T80} (*D*), anti-H4 (*F*), and anti-DM-H4 (*H*) antibodies. Nuclei are stained with DAPI. The scale bar represents 10 μm. DAPI, 4′,6-diamidino-2-phenylindole; PRMT, protein arginine methyltransferase 5; SNG, sanguinarine.

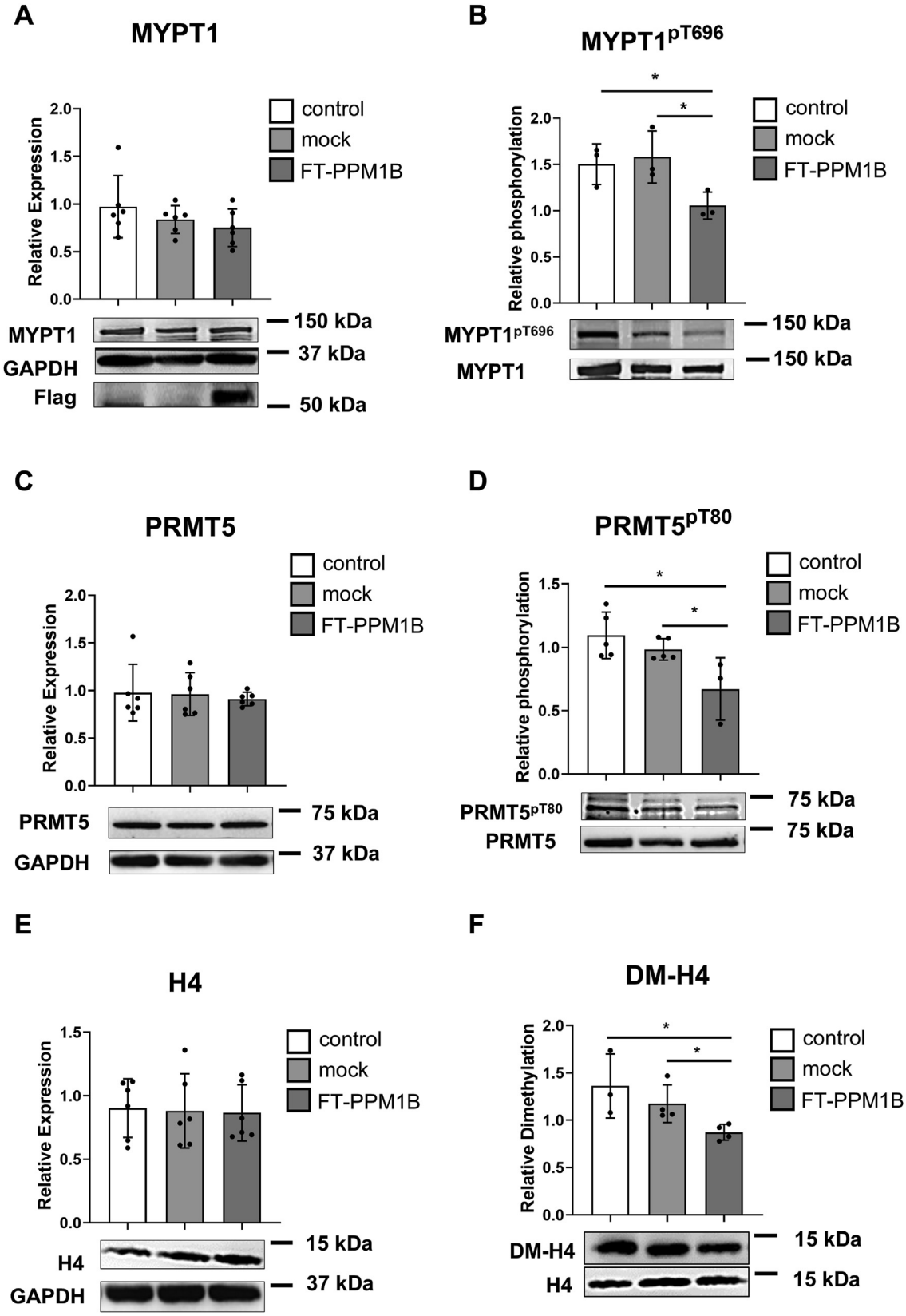

Figure 5. Effect of PPM1B overexpression on the expression and activity of MP and PRMT5. Proteins from untransfected (control), empty vector (mock), and Flag-PPM1B (FT-PPM1B) transfected HeLa cells were assessed by Western blot analysis using anti-MYPT1 (*A*), anti-MYPT1^{pT696} (*B*), anti-PRMT5 (*C*), anti-PRMT5^{pT80} (*D*), anti-H4 (*E*), and anti-DM-H4 (*F*) antibodies. Values mean ± SD, n = 3 to 6. Groups were compared using either unpaired two-tailed t-tests or one way ANOVA for comparison of multiple groups followed by Tukey *post hoc* test, where $p < 0.05$ (*). MP, myosin phosphatase; MYPT1: myosin phosphatase target subunit 1; PPM1B: protein phosphatase, Mg^{2+}/Mn^{2+} -dependent 1 B or PP2Cβ, PRMT, protein arginine methyltransferase 5.

PPM1B WT but not its phosphatase-deficient R179G mutant inhibits PRMT5 activity through the activation of myosin phosphatase

To further validate the role of PPM1B in the activation of MP by the dephosphorylation of its regulatory subunit MYPT1 on Thr 696, we generated the phosphatase deficient mutant of PPM1B (mutant R179G) based on previous publications (29). HeLa cells were transfected with the with WT (FT-PPM1B) and the phosphatase-inactive R179G mutant form of Flag-PPM1B (R179G PPM1B) and the expression and phosphorylation levels were compared to mock controls (Fig. 6). Flag tag expression compared to empty vector transfected mock control group validated successful overexpression of both mutant and WT PPM1B (Fig. 6*B*), and none of the overexpression conditions affected expression of MYPT1 (Fig. 6*A*). Phosphorylation of MYPT1 on Thr696 sidechain showed a decrease from 1.14 to 0.68 (p = 0.021) in the samples overexpressing FT-PPM1B compared to MOCK-transfected samples. In

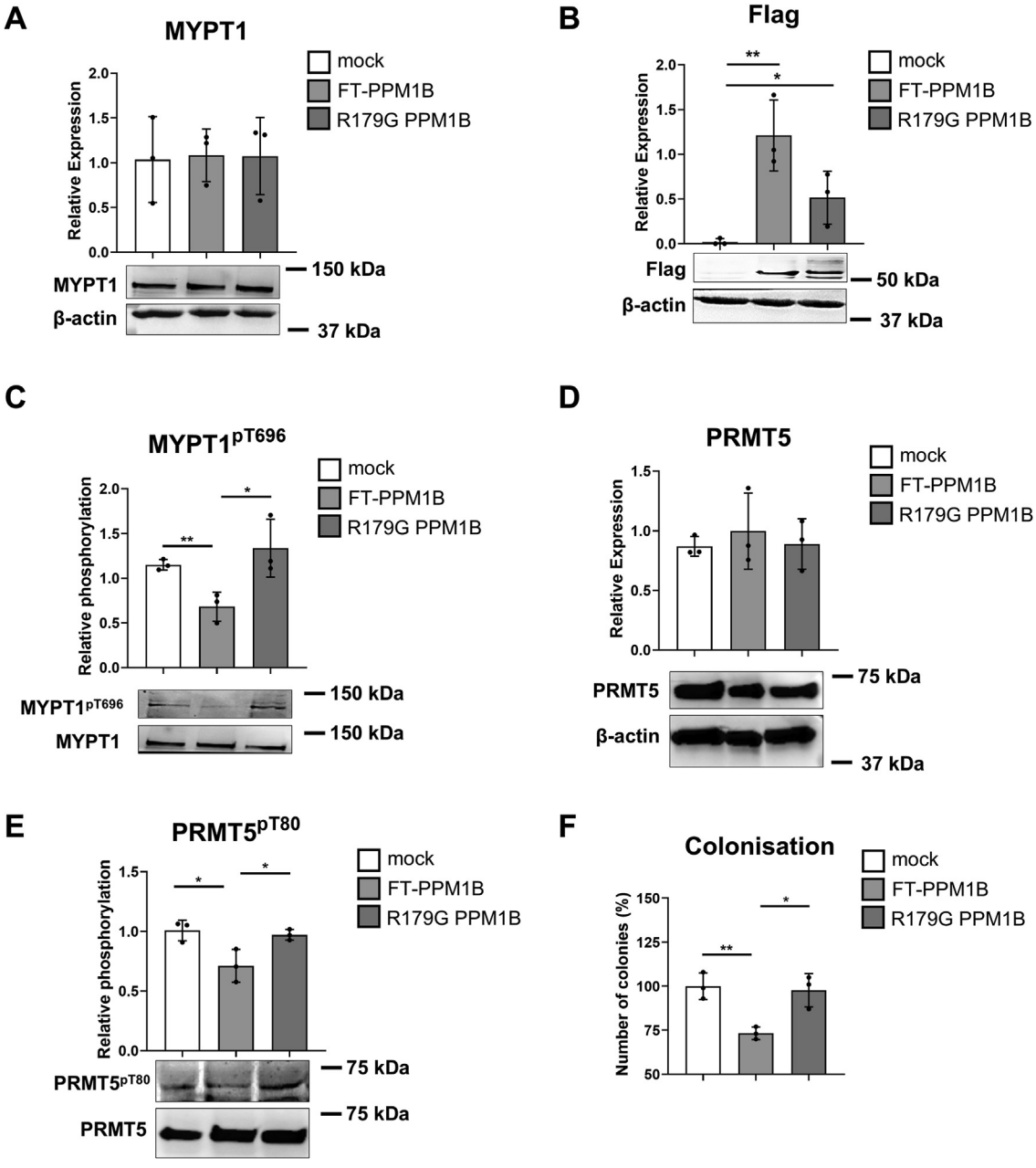

Figure 6. The effect of PPM1B^{R179G} inactive mutant on the expression and activity of MYPT1 and on the colonization capacity of HeLa cells. Proteins from empty vector (mock), WT Flag-PPM1B (WT PPM1B), and Flag-R179G inactive mutant PPM1B (R179G PPM1B) transfected HeLa cells were assessed by Western blot analysis using anti-MYPT1 (*A*), anti-Flag (*B*), anti-MYPT1^{pT696} (*C*), anti-PRMT5 (*D*), and anti-PRMT5^{pT80} (*E*) antibodies. Values are mean ± SD, n = 3. Groups were compared using either unpaired two-tailed *t* tests for comparison of two groups, or one way ANOVA for comparison of multiple groups followed by Tukey *post hoc* test, where $p < 0.05$ (*) and $p < 0.01$ (**).(*F*) Mock control, FT-PPM1B, and R179G mutant PPM1B overexpressed HeLa cells were seeded onto six well plates, and were cultured for 12 days. Survival factor was calculated and represented as *bar* chart, where values are mean ± SD, and n = 3. Groups were compared by one way ANOVA, followed by Tukey multiple comparison test, where $p < 0.05$ (*), and $p < 0.01$ (**). PRMT, protein arginine methyltransferase 5; MYPT1: myosin phosphatase target subunit 1; PPM1B, protein phosphatase, Mg^{2+}/Mn^{2+} -dependent 1 B or PP2Cβ.

addition, MYPT phosphorylation increased 1.67-fold (p = 0.0097) in the phosphatase-deficient PPM1B overexpressed samples compared to WT PPM1B values (Fig. 6*C*). The activity of the PRMT5, the substrate of MP was also affected by the overexpression of PPM1B activity. The relative phosphorylation of PRMT5 at Thr80 showed a decrease from 1.007 to 0.71 (p = 0.0022) upon the overexpression of FT-PPM1B while the overexpression of the R179G PPM1B mutant had no significant effect compared to the control (p = 0.89) but showed a 1.95-fold increase (p = 0.039) compared to the FT-PPM1B overexpressing cell lysates (Fig. 6*E*). The expression level of PRMT5 was not altered in either the FT-PPM1B or the R179G PPM1B groups compared to mock control (p = 0.77 and 0.99, respectively) (Fig. 6*D*). These results suggest the *in vivo* role of PPM1B in the dephosphorylation of MYPT1 at Thr696 inhibitory residue and its indirect effect on the activity of PRMT5.

To further investigate the difference between the effects of WT PPM1B (FT-PPM1B) and its phosphatase deficient mutant R179G overexpression, colonogenic assay for 12 days were established, in which empty vector transfected mock served as control. The colonization activity of WT PPM1B overexpressed group was reduced by 27% (p = 0.0098) compared to mock control and the overexpression of mutant R179G PPM1B elevated it back by 25% (p = 0.0150) (Fig. 6*F*) suggesting the inhibitory role of PPM1B on the colony formation of HeLa cells.

In vitro *findings of PPM1B-MYPT1-PRMT5-H4 axis are detectable in human cellular carcinoma lysates*

As our results showed the existence of the PPM1B/MP/PRMT5 axis in HeLa cervical carcinoma cells, our goal was to investigate this protooncogenic signaling pathway in human cervical carcinoma and nontumorous tissues as well. We subjected the lysates of human biopsies to semi-quantitative Western blot analysis, and cancer tissues were compared to control tissue lysates. Our results demonstrate that PPM1B and MYPT1 expression were significantly decreased to 0.44-fold (p = 0.0452) and 0.26-fold (p = 0.0244) in the tumor samples compared to the healthy control, respectively (Fig. 7, *A* and *B*). The inhibitory phosphorylation of MYPT1^{pT696} showed a strong, 2.52-fold (p = 0.0012) elevation in the tumor samples (Fig. 7*C*). PRMT5 phosphorylation on Thr^{80} residue changed significantly by 2.325-fold (p = 0.0498), while the relative PRMT5 expression decreased from 2.76 to 0.97 (p = 0.022) in the tumor samples compared to the normal samples (Fig. 7, *D* and *E*). Regarding H4, its expression showed no change (p = 0.34), while the symmetric dimethylation increased significantly by 1.327-fold (p = 0.0499) in the tumor samples compared to controls (Fig. 7, *F* and *G*). To investigate a well-known tumor suppressor that is reportedly altered by the MP/PRMT5/H4 tumorigenic pathway, we assessed pRb expression in the cervical carcinoma lysates, where expression of pRb decreased by 0.38-fold (p = 0.0435) comparing control lysates to tumorous ones (Fig. 7*H*).

Discussion

In the present study, we have characterized PPM1B as the upstream regulator of the MP/PRMT5/histone signaling pathway providing a novel mechanism of tumorigenesis in HeLa cells and cervical carcinoma. We have identified the phospho-Thr696 inhibitory residue of MYPT1 regulatory subunit of MP as the target of PPM1B. The dephosphorylation of this site was shown to decrease the activity of PRMT5, the downstream substrate of MP assessed by its regulatory Thr80 phosphorylation and histone symmetric dimethylation analysis. The interaction between MP and PPM1B was also supported by multiple interaction analyses (Fig. 1, *A–D*). The chemical inhibition of PPM1B by SNG resulted in the deactivation of MP and the increased activity of PRMT5 leading to increased symmetric dimethylation of histone H4 (Figs. 3, *A–F* and 4, *A–H*). The overexpression of the PPM1B isoform had opposite action (Fig. 5, *A–G*). The cervical carcinoma biopsies and their healthy control counterparts supported the almost complete elimination of PPM1B accompanied by tumorigenesis (Fig. 7, *A–I*). Therefore, PPM1B could be assumed as a tumor suppressor in cervical carcinoma.

We found that MP interacts with PPM1B through its MYPT1 regulatory subunit, and this interplay is supported not only by immunoprecipitation and pull-down assay but by proximity ligation assay (Fig. 1, *A–D*). It is well in line with a previous report suggesting the interaction of nuclear MYPT1 with the members of the methylosome complex as well as PPM1B isoform by mass spectrometry analysis (4). Although nuclear protein-protein interactions between the enzymes have been demonstrated, the results of the proximity ligation assay do not exclude the possibility that the interplay exists outside the nucleus and regulates possible cytosolic signal transduction processes. PPM1B exhibited cytosolic and nuclear localization, and it was supported by findings showing endogenous PPM1B localized in the nucleus of mature 3T3-L1 adipocytes where it can bind to peroxisome proliferator-activated receptor gamma (PPARγ) (30) but it was also reported as the regulator of major cytosolic signaling pathways such as mitogen-activated protein kinase and AMPK signaling (31). MYPT1 was also found in the nuclear and microsomal fraction of HepG2 cells (25) and in the nucleus of neuronal cells (32) and it was shown that nuclear MP regulated gene expression through the modulation of the PRMT5 enzyme of the methylosome complex (4).

The question arises as to what is the importance of the interaction between PPM1B and MP? The answer lies in the regulatory processes of myosin phosphatase. MYPT1 includes several consensus sites for a number of protein kinases and among these phosphorylations at Thr696 results in the inhibition of MP activity (13, 15, 33). Strikingly, none of the potent myosin phosphatase kinases is present in the nucleus (25, 34, 35). To our recent knowledge, MYPT1 is not phosphorylated in the nucleus, raising the possibility that it is translocated to the nucleus in an already phosphorylated status (36).

Our data suggest directly that MP is a substrate of PPM1B and the latter dephosphorylates the MYPT1 Thr696 inhibitory

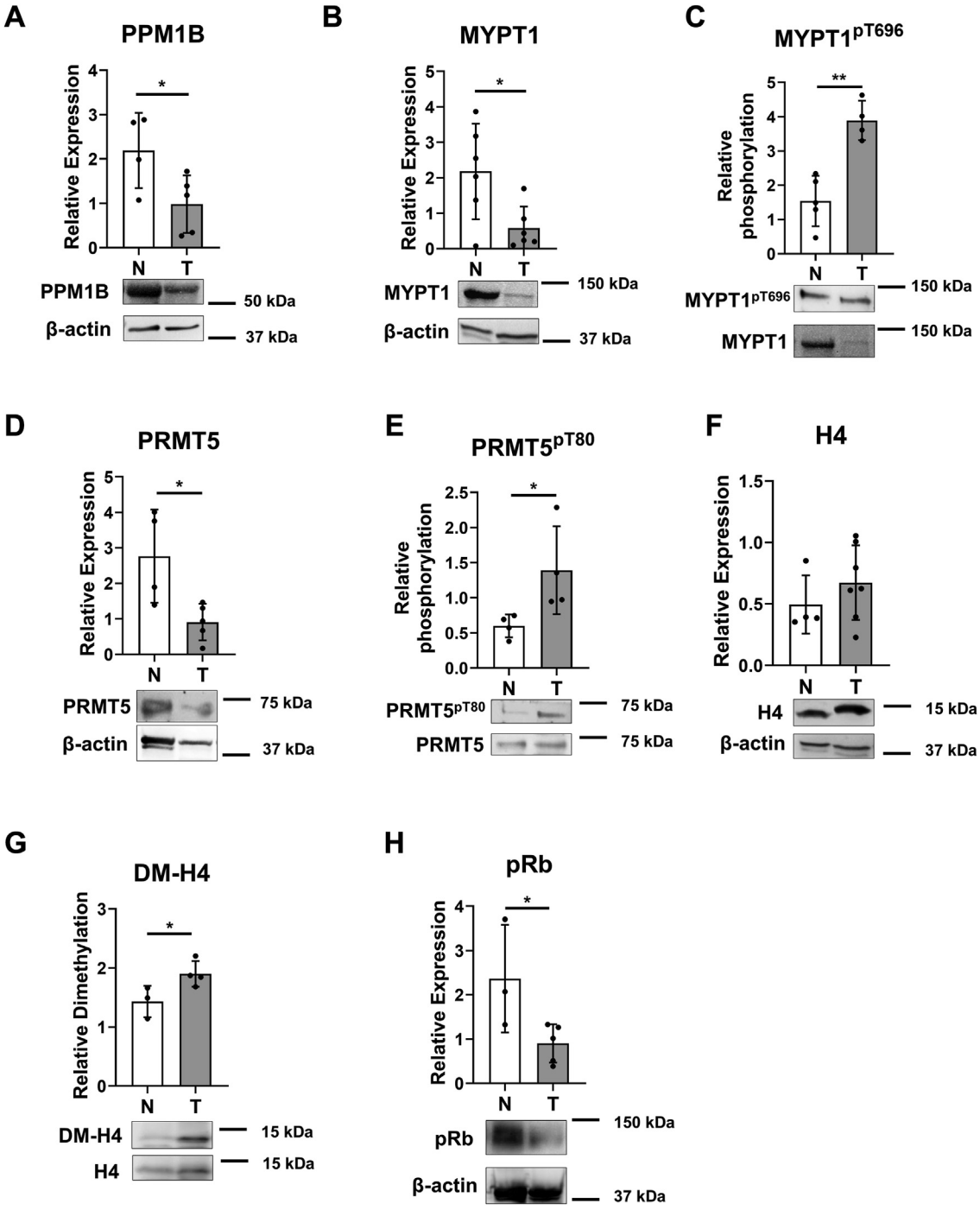

Figure 7. Expression and activity of the elements of the PPM1B/MP/PRMT5/H4 oncogenic signaling in human cervical cancer. Normal (N) and tumor (T) tissue lysates were analyzed by Western blot using anti-PPM1B (*A*), anti-MYPT1 (*B*), anti-MYPT1^{pT696} (*C*), anti-PRMT5 (*D*), anti- PRMT5^{pT80} (*E*), anti-H4 (*F*), anti-DM-H4 (*G*), and anti-pRb (*H*) antibodies. Values are mean ± SD, n = 3 to 8. Data were normalized to the healthy control. Differences between groups were analyzed by unpaired two-tailed *t* test, $p < 0.05$ (*) and $p < 0,01$ (**).MP, myosin phosphatase; MYPT1, myosin phosphatase target subunit 1; PPM1B, protein phosphatase, Mg2+/Mn2+ -dependent 1 B or PP2Cβ;pRb, retinoblastoma protein; PRMT, protein arginine methyltransferase 5.

phosphorylation site using recombinant active enzymes in *in vitro* kinase and phosphatase assays. These findings are also supported by our MP activity measurement in the presence of SNG, a PPM1 specific phosphatase inhibitor, and by *in vitro* kinase assay using ROK and recombinant active PPM1B (Fig. 2*A*). Aspecific effects beyond the inhibitory effects of SNG on PPM1 enzymes were excluded based on preliminary data, as the mitogen-activated protein kinase phosphatase-1 enzyme was only inhibited in the SNG cellular system at 17 μM IC50 value (37). Since inhibition of PPM1B did not cause a complete inhibition of MP activity, it is therefore thought that PPM1B is not the sole MYPT1 phosphatase, but rather acts in concert with other previously described regulatory protein phosphatases (17) to regulate MP holoenzyme.

The absence of PPM1 induces oncogenic signaling

Our finding that PPM1B is the major upstream regulator of nuclear MP can rely on the finding that no other protein phosphatase was present in the nuclear MYPT1 interactome (4) and the inhibitory phosphorylation levels of MYPT1 were significantly changed only in the nuclear fraction of SNG-treated HeLa cells (Fig. 3). Consistent with this, both PPM1B overexpression (Fig. 5) and chemical inhibition (Figs. 3 and 4) experiments indicate that PPM1B activates MP activity by dephosphorylating its $MYPT^{pT696}$ inhibitory phosphorylation site that results in the inhibition of PRMT5 by the decreased phosphorylation at the Thr80 activating phosphorylation site (Figs. 4*C* and 5*E*). This led to a decrease in symmetric dimethylation of histone 4 (Figs. 4*G* and 5*G*) in the nuclear fraction of HeLa cells. Our previous observations have already shown the significant upregulation of cancer-related pathways in hepatocellular carcinoma upon MYPT1 silencing that suppressed the gene and protein expression of several tumor suppressors or increased that of potential oncogenes (4).

To support our results on HeLa cells, we also analyzed the PPM1B-regulated signaling elements in human cervical tumor biopsies (Fig. 7). Recent studies have revealed tumor-suppressing roles for PPM1B; however, the Human Protein Atlas data suggested low cancer specificity. Data obtained by overexpression of WT and phosphatase dead mutant suggest that PPM1B regulates tumor cell colonization through modulation of MP and indirectly PRMT5, suggesting the tumor suppressor nature of PPM1B. (Fig. 6*F*). PPM1B inhibited gastric cancer migration and invasion *in vitro* and tumor metastasis *in vivo* by dephosphorylating Rho GDP-dissociation inhibitor (RhoGDI1) and was identified as a favorable diagnostic biomarker (28). In addition, the expression of PPM1B remarkably decreased due to the high expression of miR-186, and the overexpression of PPM1B inhibited the proliferation and tumorigenicity of bladder cancer cells (38). Moreover, the degradation of PPM1B led to the upregulation of its substrate, CDK2, and increased the proliferation and migration of hepatocellular carcinoma cells (39) and PPM1B downregulation was also was associated with more advanced clinical stages of human colorectal cancer (40). These results are fully consistent with our findings that the PPM1B expression was massively downregulated in cervical carcinoma compared to healthy controls (Fig. 7*A*).

Although most previous findings suggested the role of MP as a downstream effector of ROK signaling, more and more results suggest its ROK-independent action in the inhibition of cancer formation. The unbalanced and constant phosphorylation of MYPT1 at Thr696 was suggested to be related to cancer formation and mutations as well as altered phosphorylation and expression of MYPT1 were documented in various cancer types (14). Interestingly, decreased expression of MYPT1 did not always accompany tumor development, but increased phosphorylation of MYPT. This phenomenon may be explained, at least in part, by the regulation of MP with PPM1B. Interestingly, in those cancer types where PPM1B downregulation was detected such as bladder, gastric, and hepatocellular carcinoma, only the inhibitory phosphorylation of MYPT1 showed correlation but not the MYPT1 protein expression (4) which explains the tumor suppressor activity of MP without any changes in its protein expression. Although this is a favorable explanation, the possibility of regulation by miRNA cannot be ruled out.

Taken together, the present study has identified PPM1B as a novel phosphatase of MP and as an upstream regulator of the MP/PRMT5/histone signaling pathway. It provides new insight into the molecular mechanism by which PPM1B regulates cancer cell formation through activation of myosin phosphatase. MP and PPM1B clearly serve tumor suppressive functions, and are inactivated in human cancer patients. Beyond their prognostic feature in most cancer types—such as in cervical carcinoma—their reactivation by small pharmacologic compounds is rather important but remains challenging. The mere inhibition of the upstream kinases is not sufficient, but also requires the activation of counteracting phosphatase(s) in targeting oncogenic phosphorylations to increase the efficiency of kinase inhibitor therapies.

Experimental procedures

Chemicals

All chemicals were obtained from Sigma-Aldrich unless indicated otherwise.

Antibodies

All antibodies are described in Table S1.

Cell culture maintenance

Human epithelioid cervix carcinoma HeLa cell line and SV40 transformed human embryonal kidney cells (purchased from ECACC, cat. number 99040201 and 85120602, respectively), were maintained according to the manufacturer's instructions in Dulbecco's modified Eagle's medium (DMEM) with phenol red, supplemented by 10% fetal bovine serum (FBS), and 2 mM L-glutamine (further referred as complete growth medium). Cells were incubated at 37 °C in a humidified atmosphere containing 5% CO_2. Cell lines were tested for *mycoplasma* and they were free from *mycoplasma* contamination for all experiments. The authenticity of the cell lines were validated and documented by the manufacturer. Cell lines were tested and they were free from *mycoplasma* contamination for all experiments.

Overexpression of PPM1B protein

Mg^{2+}/Mn^{2+} dependent protein phosphatase 1B (PPM1B) was overexpressed in HeLa cells using 1.7 ng/µl human pReceiver-M11-FT-PPM1B plasmid (GeneCopoeia) and Gene Juice transfection reagent (5.32 µg dissolved in 1500 µl serum free DMEM) according to the manufacturer's protocol (labeled as FT-PPM1B group). Mock control group was established by the same amount of transfection reagent and equal concentration of empty vector (further referred as mock group). Cells were cultured for 72 h after transfection then lysed as it is described in "Protein extraction" section.

Site-directed mutagenesis of R179G inactive mutant of PPM1B

Expression vector pReceiver-M11 encoding WT human full-length PPM1B (NM_002706.6) transcript variant 1 was purchased from GeneCopoeia Inc. Point mutations of PPM1BR179G/pReceiver-M11 were performed using QuickChange II XL Site-Directed Mutagenesis Kit according to the manufacturer's instructions (Agilent Technologies) and is further referred to as R179G mutant PPM1B. Primer pairs are listed in Table S2. The sequence of mutants was verified by DNA sequencing, performed by GenoMed Medical Genomic Technologies Ltd. Primers for sequencing are listed in Table S2. Vectors containing mutant protein sequence were produced by *Escherichia coli* cultures then HeLa cells were transfected with the mutant plasmid with the same conditions as described in the "Overexpression of PPM1B protein" section.

SNG treatment and subcellular fractionation

Prior to SNG treatment, HeLa cell culture was incubated in incomplete DMEM containing 0.1% FBS for 24 h and then treated with 1 μM SNG dissolved in complete media for 1 h to inhibit the activity of PPM1B. Serum-starved cells without any treatment served as the control group. Cells were either processed according to the protocol described in "Protein Extraction" section or were handled as follows. Cells were washed with 1x PBS, then centrifuged at 800*g* for 3 min and were solubilized in 400 μl of "Buffer A" consisting of: 10 mM 4-(2-hydroxyethyl)-1-piperazineethanesulphonic acid (Hepes pH 7.9), 10 mM potassium chloride (KCl), 0.1 mM EDTA, 0.1 mM ethylene glycol-bis(β-aminoethyl ether)-N,N,N′,N′-tetraacetic acid (EGTA) supplemented with 1 mM DTT, and 10x dilution of phosphatase inhibitor cocktail (1 mM sodium fluoride (NaF), 1 mM tetrasodium pyrophosphate ($Na_4P_2O_7$), 1 mM β-glycerophosphate, and 1 mM sodium orthovanadate (Na_3VO_4), mixture further referred to as 10x phosphatase inhibitor cocktail (PIC)) plus 1 μM Microcystin-LR (McαR). Samples were homogenized using Hamilton needle, then the mixture was centrifuged at 16,000*g* for 1 min, and the supernatant was saved as the cytoplasmic fraction. The pellet was suspended in 50 μl "Buffer B" (20 mM Hepes pH 7.9, 420 mM sodium chloride (NaCl), 0.5 mM EDTA, and 0.5 mM EGTA) supplemented by 10xPIC and 1 μM McαR as described above, then the mixture was incubated on ice for 25 min and centrifuged at 12,000*g* for 10 min. The supernatants were considered as nuclear fraction. Protein concentrations were determined with Pierce BCA Protein Assay Kit (Thermo Fisher Scientific,) as described before (32).

Protein extraction

Cells were washed once with 1xPBS (pH 7.4) and then lysed in radioimmunoprecipitation assay buffer (25 mM Tris, 150 mM NaCl, 1% Na-deoxycholate, 0.1% SDS) supplemented with 1% Triton-X-100, protease inhibitor, and PIC. Proteins were solubilized by sonication and were centrifuged at 13,000*g* at 4 °C for 10 min, supernatant was considered as total protein extract. Protein concentrations were determined with Pierce BCA Protein Assay Kit (Thermo Fisher Scientific) as described before (32).

Alamar Blue cell viability assay

HeLa cells were plated on 96-well plates and were transfected by FT-PPM1B as described above, and were incubated for 72 h, or were grown for 24 h, then serum starved in 0.1% FBS-containing media for 24 h prior to 1 h long 1 μM SNG treatment. Then, resazurin was added at a 20 μM final concentration for 2 h, and the fluorescence intensity was measured using a Tecan Spark 10M multimode plate reader (Tecan Group Ltd) at 560/590 nm. Viability was expressed as the percentage of untreated cells.

Human cervix tissue lysates

Normal and tumor tissue lysates were obtained from Protein Biotechnologies solubilized in radioimmunoprecipitation assay buffer. After centrifugation at 16,000*g*, at 4 °C for 4 min, supernatants were incubated in SDS sample buffer (Bio-Rad Laboratories) for 5 min at 100 °C and the samples were applied for Western blot analysis.

Western blot analysis

Lysates (20 μg of protein per sample) were loaded onto 4 to 20% precast Criterion gels (Bio-Rad Laboratories) and were separated by size, then transferred to nitrocellulose membrane at 200 V as described previously using a Criterion blotter (Bio-Rad Laboratories) at 100 V for 75 min and handled as described previously (41). Bands were visualized in a ChemiDoc Touch Imaging System (Bio-Rad Laboratories) using Western Bright enhanced chemiluminescence reagents (Advansta Inc).

Immunofluorescent staining and confocal microscopy by high content screening

HeLa cells were added to 96-well Cell Carrier Ultra glass bottom plates (PerkinElmer) for 24 h then were incubated in 0.1% FBS-containing DMEM for 24 h followed by treatment with 1 μM SNG for 1 h. In case of PPM1B overexpression, cells were transfected as described previously. In both cases untreated cells served as control group. Cells were fixed with 300 μl/well 4% (v/v) paraformaldehyde/Tris-buffered saline (TBS) (50 mM Tris, pH 7.4, 150 mM NaCl, 1 mM EDTA, 1x PIC, 1x phosphatase inhibitor cocktail, 1% (v/v) Triton X-100) for 10 min at room temperature (RT), permeabilized with 300 μl/well 0.25% Triton X-100/TBS solution for 15 min and the nonspecific binding sites were blocked with 300 μl/well 1% bovine serum albumin (BSA)/TBS solution for 1 h. After blocking, the cells were labeled with antibodies raised against MYPT1, MYPT1^{pT696}, PRMT5, PRMT5^{pT80}, H4, dimethyl-H4, PPM1B, or Flag antibodies in 1:100 dilution in blocking solution at 4 °C overnight, followed by Alexa Fluor 488-conjugated chicken anti-rabbit or anti-mouse antibody in 1:1000 dilution in blocking solution for 1.5 h at RT. Actin was visualized by Texas Red Phalloidin and nuclei were stained with DAPI for 2 min. Finally, the cells were washed three times with 1xPBS. The visualization was conducted in each case by

Opera Phenix High Content Analysis equipment (PerkinElmer) using a 40x water objective in confocal mode. The nuclear region of the cells was segmented based on DAPI staining and was analyzed with the built-in Harmony software (version 4.8; http://www.perkinelmer.com/product/harmony-4-2office-hh17000001).

Immunoprecipitation

Flag-PPM1B (FT-PPM1B) and Flag-MYPT1 (FT-MYPT1) proteins were expressed in tsA201 cell line as described before, and cells were lysed in TBS-EDTA buffer. PAS) resin (GE HealthCare, #17–0780–01) was blocked with 5% (w/V) BSA/TBS for one night (∼16 h) at 4 °C. Then antibodies (anti-PPM1B, anti-MYPT1, or anti-mouse) were coupled to PAS in binding buffer (50 mM Tris, pH 7.0) in 1:67 dilution by gentle rotation for 3 h at 4 °C. The tsA201 lysates (1 mg/ml) were precleared with PAS and then were added to the PAS-antibody complex for 2 h and were washed three times with 1xTBS. Then PAS-anti-MYPT1-FT-MYPT1 particles were incubated with FT-PPM1B containing precleared tsA201 lysate, while PAS-anti-PPM1B-FT-PPM1B complexes with FT-MYPT1 for 3 h. Finally, beads were washed with 1xTBS and were incubated at 100 °C for 5 min in 1x SDS sample buffer. Samples were investigated by SDS-PAGE followed by Western blot analysis.

Pull-down assay

Glutathione Sepharose 4B beads (P1743-1VL, Merck) (30 μl/sample) were incubated with 400 μl binding buffer (50 mM Tris, 150 mM NaCl, 1 mM EDTA, 1% (V/V) Triton X-100, pH 7.4, and 1 x PIC) containing 1 μM purified GST or GST-MYPT1 in for 60 min at 4 °C. The resin-GST/GST-MYPT1 complexes were washed with TBS and then were incubated either with untransfected or Flag-PPM1B over-expressing tsA201 lysates (previously precleared with uncoupled Glutathione Sepharose 4B) for 120 min at 4 °C. The resins were washed three times with TBS then incubated with 2x SDS sample buffer for 5 min at 100 °C (32). The samples were analyzed by Western blotting using antibodies against PPM1B, PP1c, and GST. GST-MYPT1 were expressed in *E. coli* and purified as described before (42, 43).

Duolink PLA protein-protein interaction assay

Duolink PLA protein-protein interaction assay (DUO92007, Sigma-Aldrich) was conducted according to the instructions of the manufacturer. Cells were plated on CellCarrier Ultra glass bottom plates (PerkinElmer), and were fixed by 300 μl/well 4%(v/v) paraformaldehyde/TBS, and permeabilized in 300 μl/well 0.2% Triton-X-100 in TBS. Samples were incubated with primary antibodies in 1:100 dilution, specific for MYPT1 and PPM1B, or with anti-PP1cβ and anti-MYPT1 for positive control group, or with anti-pRb and anti-MYPT1 and with anti-PPM1A and anti-MYPT1. In negative control group no primary antibodies were applied. Total volume used of the primary antibody was 100 μl/well, and the samples were incubated for O/N at 4 °C. Duolink PLA probe was then ligated to primary antibodies, and then amplification buffer was added to the system in 40 μl/well volume, enabling fluorescent oligonucleotide sequences to be polymerized in between PLA probes linked to proteins by primary antibodies, which were in optimal physical proximity to each other. Fluorescent signal of polymerized oligonucleotides was read by Opera Phoenix High Content Screening instrument built-in Harmony software (version 4.8), at an excitation of 554 nm, and emission of 576 nm, by 40x water objective. Registered signals of interacting proteins showed up as fluorescent spots. To determine cell area and nuclei area, cytoplasm and nuclei were stained by Alexa688 Phalloidin and DAPI, respectively. Fluorescent spots indicating the interactions were counted and determined by built in intelligent Harmony software (version 4.8), and the spot number was normalized to cell number obtained by DAPI nuclei staining. For each interaction group at least triplicates of wells were visualized, by at least 9 pixels per well density. Negative control group values were expressed as spot/cell, and were taken as 100%. The values of all other groups were taken as a ratio to the control value.

Assay of MP activity

HeLa cells were subcultured then serum starved in 0.1% FBS DMEM for 24 h then were treated with 1 μM SNG or 50 nM OA, as well as combined treatments with 50 nM OA and 1 μM SNG suspended in complete media for 1 h. Cells were washed and lysed in 50 mM Tris–HCl pH 7.4, 150 mM NaCl, 0.15%(m/V) buffer with 1x PIC, 1 mM PMSF, and 50 mM 2-mercaptoethanol with ultrasound. After centrifugation (16,000*g*, 20 min), the supernatants were preincubated for 1 min at 30 °C and assayed in presence of 1 μM phosphorylated smooth muscle myosin substrate (^{32}P-myosin) for 1 min as described earlier (25). The values were normalized to the MYPT1 content of the samples assessed by a standard curve using GST-MYPT1 recombinant protein. MP activity values were expressed as ratio to the control group. Columns represent mean ± SD, n = 3. Comparison of groups were conducted by one-way ANOVA with Tukey post hoc analysis, and two samples were compared by unpaired two-tailed *t* test, where statistical significance was validated upon $p < 0.05$.

RhoA kinase assay and PPM1B phosphatase assay

Glutathione Sepharose 4B beads (30 μl/sample) coupled with GST or GST-MYPT1 were washed with TBS and incubated with ROK (20 ng/μl) and ATP (1 mM) for 45 min at 30 °C in ROK assay buffer (20 mM Mops pH 7.2 25 mM GlicP, 0.5 mM EGTA, 5 mM $MgCl_2$, and 0.5 mM DTT) in the presence of 1 μM of McαR and 1 x PIC. Control samples were handled in the same way without the addition of ROK. After phosphorylation, the beads were washed three times with TBS and incubated in the presence or absence of PPM1B in a buffer containing 20 mM Tris pH 7.4, 150 mM NaCl, 1 mM DTT, 1 mg/ml BSA, 0.1% Tween, protease inhibitors, 5 mM $MgCl_2$, and 5 mM $MnCl_2$ for 45 min at 30 °C. PPM1B activity was also tested in the presence of 1 μM SNG or without the addition of $MgCl_2$ and $MnCl_2$. After washing with TBS, beads were incubated with SDS sample buffer at 100 °C for 5 min.

Phosphorylation level of MYPT1 were analyzed by Western blot using MYPT1-^{pT853} and MYPT1-^{pT696} phospho-specific antibodies and anti-MYPT1 as a loading control.

Colonogenic assay

HeLa cells were seeded at a density of 10^3 cells/well in six well plates, and were transfected as it was previously described, either with FT-PPM1B (WT PPM1B) or R179G mutant PPM1B (inactive phosphatase) plasmid. Empty vector treated mock served as control. Cells were cultured for 12 days, after which cultures were washed with 1X PBS, and were dried at RT for 30 min. Cells were stained with 0.27 m/m% Coomassie Brilliant Blue R250 dye (B0149), were visualized, and colonies were counted by ImageJ software (https://imagej.net/ij/). Colony numbers were normalized to plated cell number. The average colony number of Mock groups was taken as 100%, and all other groups were expressed as ratio and results were represented as bar charts.

Statistical analysis

Immunoblots were analyzed by ImageJ software. All data were represented as bar charts, created by GraphPad Prism 8 software. Statistical analyses were also performed using GraphPad Prism 8 software (https://www.graphpad.com/updates/prism-10-1-1-release-notes). Phosphorylated proteins were normalized to non-phosphorylated protein expression, and expressed as relative numbers, while nonphosphorylated protein expression was normalized to the loading control, either GAPDH or β-actin, and were represented as relative numbers, except for SNG treatment, where raw data are presented for total proteins. Results of MP activity, Duolink, Alamar Blue viability, and Colonogenic assay values were expressed as ratio to the control group. All data are presented as mean ± SD, where n is the number of independently performed experiments. Differences were considered statistically significant at $p < 0.05$ using unpaired two-tailed t tests to compare two groups, and one-way or two-way ANOVA to compare multiple groups, followed by Tukey multiple comparison test. Data were tested for normal distribution and outliers were defined by Grubbs's test.

Data availability

All data are contained within the manuscript. Data are to be shared upon request (contact: lontay@med.unideb.hu). No datasets were deposited into a publicly accessible repository.

Supporting information—This article contains supporting information.

Acknowledgments—We thank Andrea Docsa and Ágota Kelemenné Szántó for their excellent technical assistance and for Vy Nhat Huynh for his technical help to cell viability assay.

Author contributions—I. K., A. U., E. M., D. H, Z. K., E. T., A. K., and B. L. methodology; I. K., A. U., and Z. K. investigation; I. K. and A. U., software; I. K., E. M., and D. H., validation; I. K., E. M., F. E., A. K. and B. L. writing–review and editing; I. K., Z. K., A. K., and B. L. formal analysis; I. K., A. U., and E. T. visualization; I. K. and B. L. data curation; I. K. and B. L. writing–original draft; I. K. project administration; B. L. funding acquisition; B. L. conceptualization.

Funding and additional information—This work was supported by grants from the National Research, Development and Innovation Office FK125043 and K143430 (to B. L), K129104 (to F. E), the University of Debrecen, Faculty of Medicine Research Fund (1G3DBKJ0BFTK247).

Conflict of interest—The authors declare that they have no conflicts of interest with the contents of this article.

Abbreviations—The abbreviations used are: BSA, bovine serum albumin; DAPI, 4′,6-diamidino-2-phenylindole; DMEM, Dulbecco's modified Eagle's medium; EGTA, ethylene glycol-bis(β-aminoethyl ether)-N,N,N′,N′-tetraacetic acid; FBS, fetal bovine serum; MP, myosin phosphatase; MYPT1, myosin phosphatase target subunit 1; OA, okadaic acid; PAS, protein A sepharose; PIC, phosphatase inhibitor cocktail; PLA, proximity ligation assay; PP1c, protein phosphatase 1 catalytic subunit; PPM1, Mg^{2+}/Mn^{2+} dependent protein phosphatase M1; PPM1A, protein phosphatase, $Mg^{2+/}Mn^{2+}$ -dependent 1 A or PP2Cα; PPM1B, protein phosphatase, $Mg^{2+/}Mn^{2+}$ -dependent 1 B or PP2Cβ; PPP1CB, protein phosphatase catalytic subunit β/δ isoform or PP1c; pRb, retinoblastoma protein; PRMT5, protein arginine methyltransferase 5; ROK, Rho A activated kinase; RT, room temperature; SNG, sanguinarine; TBS, Tis-buffered saline.

References

1. Tsang, D. P., and Cheng, A. S. (2011) Epigenetic regulation of signaling pathways in cancer: role of the histone methyltransferase EZH2. *J. Gastroenterol. Hepatol.* **26**, 19–27
2. Geffen, Y., Anand, S., Akiyama, Y., Yaron, T. M., Song, Y., Johnson, J. L., *et al.* (2023) Pan-cancer analysis of post-translational modifications reveals shared patterns of protein regulation. *Cell* **186**, 3945–3967. e3926
3. Wang, H., Yang, L., Liu, M., and Luo, J. (2023) Protein post-translational modifications in the regulation of cancer hallmarks. *Cancer Gene Ther.* **30**, 529–547
4. Sipos, A., Ivan, J., Becsi, B., Darula, Z., Tamas, I., Horvath, D., *et al.* (2017) Myosin phosphatase and RhoA-activated kinase modulate arginine methylation by the regulation of protein arginine methyltransferase 5 in hepatocellular carcinoma cells. *Sci. Rep.* **7**, 40590
5. Kim, H., and Ronai, Z. A. (2020) PRMT5 function and targeting in cancer. *Cell Stress* **4**, 199–215
6. Al-Hamashi, A. A., Diaz, K., and Huang, R. (2020) Non-histone arginine methylation by protein arginine methyltransferases. *Curr. Protein Pept. Sci.* **21**, 699–712
7. Antonysamy, S., Bonday, Z., Campbell, R. M., Doyle, B., Druzina, Z., Gheyi, T., *et al.* (2012) Crystal structure of the human PRMT5:MEP50 complex. *Proc. Natl. Acad. Sci. U. S. A.* **109**, 17960–17965
8. Ho, M. C., Wilczek, C., Bonanno, J. B., Xing, L., Seznec, J., Matsui, T., *et al.* (2013) Structure of the arginine methyltransferase PRMT5-MEP50 reveals a mechanism for substrate specificity. *PLoS One* **8**, e57008
9. Stopa, N., Krebs, J. E., and Shechter, D. (2015) The PRMT5 arginine methyltransferase: many roles in development, cancer and beyond. *Cell. Mol. Life. Sci.* **72**, 2041–2059
10. Lattouf, H., Kassem, L., Jacquemetton, J., Choucair, A., Poulard, C., Tredan, O., *et al.* (2019) LKB1 regulates PRMT5 activity in breast cancer. *Int. J. Cancer* **144**, 595–606
11. Liu, F., Zhao, X., Perna, F., Wang, L., Koppikar, P., Abdel-Wahab, O., *et al.* (2011) JAK2V617F-mediated phosphorylation of PRMT5

downregulates its methyltransferase activity and promotes myeloproliferation. *Cancer Cell* **19**, 283–294
12. Zhu, F., and Rui, L. (2019) PRMT5 in gene regulation and hematologic malignancies. *Genes Dis.* **6**, 247–257
13. Hartshorne, D. J., Ito, M., and Erdodi, F. (1998) Myosin light chain phosphatase: subunit composition, interactions and regulation. *J. Muscle Res. Cell Motil* **19**, 325–341
14. Kiss, A., Erdodi, F., and Lontay, B. (2019) Myosin phosphatase: unexpected functions of a long-known enzyme. *Biochim. Biophys. Acta Mol. Cell Res* **1866**, 2–15
15. Kimura, K., Ito, M., Amano, M., Chihara, K., Fukata, Y., Nakafuku, M., *et al.* (1996) Regulation of myosin phosphatase by Rho and rho-associated kinase (Rho-kinase). *Science* **273**, 245–248
16. Feng, J., Ito, M., Ichikawa, K., Isaka, N., Nishikawa, M., Hartshorne, D. J., *et al.* (1999) Inhibitory phosphorylation site for Rho-associated kinase on smooth muscle myosin phosphatase. *J. Biol. Chem.* **274**, 37385–37390
17. Muranyi, A., Derkach, D., Erdodi, F., Kiss, A., Ito, M., and Hartshorne, D. J. (2005) Phosphorylation of Thr695 and Thr850 on the myosin phosphatase target subunit: inhibitory effects and occurrence in A7r5 cells. *FEBS Lett.* **579**, 6611–6615
18. Khasnis, M., Nakatomi, A., Gumpper, K., and Eto, M. (2014) Reconstituted human myosin light chain phosphatase reveals distinct roles of two inhibitory phosphorylation sites of the regulatory subunit, MYPT1. *Biochemistry* **53**, 2701–2709
19. Ichikawa, K., Ito, M., and Hartshorne, D. J. (1996) Phosphorylation of the large subunit of myosin phosphatase and inhibition of phosphatase activity. *J. Biol. Chem.* **271**, 4733–4740
20. Lontay, B., Pal, B., Serfozo, Z., Koszeghy, A., Szucs, G., Rusznak, Z., *et al.* (2012) Protein phosphatase-1M and Rho-kinase affect exocytosis from cortical synaptosomes and influence neurotransmission at a glutamatergic giant synapse of the rat auditory system. *J. Neurochem.* **123**, 84–99
21. Aburai, N., Yoshida, M., Ohnishi, M., and Kimura, K. (2010) Sanguinarine as a potent and specific inhibitor of protein phosphatase 2C in vitro and induces apoptosis via phosphorylation of p38 in HL60 cells. *Biosci. Biotechnol. Biochem.* **74**, 548–552
22. Yu, Y., Luo, Y., Fang, Z., Teng, W., Yu, Y., Tian, J., *et al.* (2020) Mechanism of sanguinarine in inhibiting macrophages to promote metastasis and proliferation of lung cancer via modulating the exosomes in A549 cells. *Onco Targets Ther.* **13**, 8989–9003
23. Wu, Y., Erdodi, F., Muranyi, A., Nullmeyer, K. D., Lynch, R. M., and Hartshorne, D. J. (2003) Myosin phosphatase and myosin phosphorylation in differentiating C2C12 cells. *J. Muscle Res. Cell Motil* **24**, 499–511
24. Alessi, D., MacDougall, L. K., Sola, M. M., Ikebe, M., and Cohen, P. (1992) The control of protein phosphatase-1 by targetting subunits. The major myosin phosphatase in avian smooth muscle is a novel form of protein phosphatase-1. *Eur. J. Biochem.* **210**, 1023–1035
25. Lontay, B., Kiss, A., Gergely, P., Hartshorne, D. J., and Erdodi, F. (2005) Okadaic acid induces phosphorylation and translocation of myosin phosphatase target subunit 1 influencing myosin phosphorylation, stress fiber assembly and cell migration in HepG2 cells. *Cell Signal* **17**, 1265–1275
26. Favre, B., Turowski, P., and Hemmings, B. A. (1997) Differential inhibition and posttranslational modification of protein phosphatase 1 and 2A in MCF7 cells treated with calyculin-A, okadaic acid, and tautomycin. *J. Biol. Chem.* **272**, 13856–13863
27. Lontay, B., Bodoor, K., Sipos, A., Weitzel, D. H., Loiselle, D., Safi, R., *et al.* (2015) Pregnancy and smoothelin-like protein 1 (SMTNL1) deletion promote the switching of skeletal muscle to a glycolytic phenotype in human and mice. *J. Biol. Chem.* **290**, 17985–17998
28. Li, R., Dou, J., Bai, T., Cai, B., and Liu, Y. (2022) Protein phosphatase PPM1B inhibits gastric cancer progression and serves as a favorable prognostic biomarker. *Appl. Immunohistochem. Mol. Morphol.* **30**, 366–374
29. Zhao, Y., Liang, L., Fan, Y., Sun, S., An, L., Shi, Z., *et al.* (2012) PPM1B negatively regulates antiviral response via dephosphorylating TBK1. *Cell. Signal.* **24**, 2197–2204
30. Tasdelen, I., van Beekum, O., Gorbenko, O., Fleskens, V., van den Broek, N. J., Koppen, A., *et al.* (2013) The serine/threonine phosphatase PPM1B (PP2Cbeta) selectively modulates PPARgamma activity. *Biochem. J.* **451**, 45–53
31. Li, Z., Chen, R., Li, Y., Zhou, Q., Zhao, H., Zeng, K., *et al.* (2023) A comprehensive overview of PPM1B: from biological functions to diseases. *Eur. J. Pharmacol.* **947**, 175633
32. Lontay, B., Serfozo, Z., Gergely, P., Ito, M., Hartshorne, D. J., and Erdodi, F. (2004) Localization of myosin phosphatase target subunit 1 in rat brain and in primary cultures of neuronal cells. *J. Comp. Neurol.* **478**, 72–87
33. Broustas, C. G., Grammatikakis, N., Eto, M., Dent, P., Brautigan, D. L., and Kasid, U. (2002) Phosphorylation of the myosin-binding subunit of myosin phosphatase by Raf-1 and inhibition of phosphatase activity. *J. Biol. Chem.* **277**, 3053–3059
34. Acconcia, F., Barnes, C. J., Singh, R. R., Talukder, A. H., and Kumar, R. (2007) Phosphorylation-dependent regulation of nuclear localization and functions of integrin-linked kinase. *Proc. Natl. Acad. Sci. U. S. A.* **104**, 6782–6787
35. Surve, S. V., Myers, P. J., Clayton, S. A., Watkins, S. C., Lazzara, M. J., and Sorkin, A. (2019) Localization dynamics of endogenous fluorescently labeled RAF1 in EGF-stimulated cells. *Mol. Biol. Cell* **30**, 506–523
36. Ryan, T., Shelton, M., Lambert, J. P., Malecova, B., Boisvenue, S., Ruel, M., *et al.* (2013) Myosin phosphatase modulates the cardiac cell fate by regulating the subcellular localization of Nkx2.5 in a Wnt/Rho-associated protein kinase-dependent pathway. *Circ. Res.* **112**, 257–266
37. Vogt, A., Tamewitz, A., Skoko, J., Sikorski, R. P., Giuliano, K. A., and Lazo, J. S. (2005) The benzo[c]phenanthridine alkaloid, sanguinarine, is a selective, cell-active inhibitor of mitogen-activated protein kinase phosphatase-1. *J. Biol. Chem.* **280**, 19078–19086
38. Yang, Z., Xu, G., Wang, B., Liu, Y., Zhang, L., Jing, T., *et al.* (2021) USP12 downregulation orchestrates a protumourigenic microenvironment and enhances lung tumour resistance to PD-1 blockade. *Nat. Commun.* **12**, 4852
39. Ying, H., Ji, L., Xu, Z., Fan, X., Tong, Y., Liu, H., *et al.* (2020) TRIM59 promotes tumor growth in hepatocellular carcinoma and regulates the cell cycle by degradation of protein phosphatase 1B. *Cancer Lett.* **473**, 13–24
40. Wang, H., Chen, Y., Han, J., Meng, Q., Xi, Q., Wu, G., *et al.* (2016) DCAF4L2 promotes colorectal cancer invasion and metastasis via mediating degradation of NFkappab negative regulator PPM1B. *Am. J. Transl Res.* **8**, 405–418
41. Horvath, D., Sipos, A., Major, E., Konya, Z., Batori, R., Dedinszki, D., *et al.* (2018) Myosin phosphatase accelerates cutaneous wound healing by regulating migration and differentiation of epidermal keratinocytes via Akt signaling pathway in human and murine skin. *Biochim. Biophys. Acta Mol. Basis Dis.* **1864**, 3268–3280
42. Kiss, E., Muranyi, A., Csortos, C., Gergely, P., Ito, M., Hartshorne, D. J., *et al.* (2002) Integrin-linked kinase phosphorylates the myosin phosphatase target subunit at the inhibitory site in platelet cytoskeleton. *Biochem. J.* **365**, 79–87
43. Toth, A., Kiss, E., Herberg, F. W., Gergely, P., Hartshorne, D. J., and Erdodi, F. (2000) Study of the subunit interactions in myosin phosphatase by surface plasmon resonance. *Eur. J. Biochem.* **267**, 1687–1697